REPORT DOCUMENTATION PAGE

Form Approved
OMB No. 0704-0188

The public reporting burden for this collection of information is estimated to average 1 hour per response, including the time for reviewing instructions, searching existing data sources, gathering and maintaining the data needed, and completing and reviewing the collection of information. Send comments regarding this burden estimate or any other aspect of this collection of information, including suggestions for reducing the burden, to Department of Defense, Washington Headquarters Services, Directorate for Information Operations and Reports (0704-0188), 1215 Jefferson Davis Highway, Suite 1204, Arlington, VA 22202-4302. Respondents should be aware that notwithstanding any other provision of law, no person shall be subject to any penalty for failing to comply with a collection of information if it does not display a currently valid OMB control number.

PLEASE DO NOT RETURN YOUR FORM TO THE ABOVE ADDRESS.

1. REPORT DATE *(DD-MM-YYYY)*	2. REPORT TYPE	3. DATES COVERED *(From - To)*
4-6-2012	Phase I Final	18th March 2010 - 18th May 2012

4. TITLE AND SUBTITLE

Coherent Distributed Radar for High-Resolution Through-Wall Imaging

5a. CONTRACT NUMBER

N00014-10-C-0277

5b. GRANT NUMBER

5c. PROGRAM ELEMENT NUMBER

6. AUTHOR(S)

Eric van Doorn, Ph.D. (PI)
Satya Ponnaluri, Ph.D.

5d. PROJECT NUMBER

5e. TASK NUMBER

5f. WORK UNIT NUMBER

7. PERFORMING ORGANIZATION NAME(S) AND ADDRESS(ES)

Intelligent Automation, Inc.
15400 Calhoun Drive, Suite 400
Rockville, MD 20855

8. PERFORMING ORGANIZATION REPORT NUMBER

9. SPONSORING/MONITORING AGENCY NAME(S) AND ADDRESS(ES)

Naval Research Lab
4555 Overlook Avenue, SW
Washington, DC 20375-5320

10. SPONSOR/MONITOR'S ACRONYM(S)

11. SPONSOR/MONITOR'S REPORT NUMBER(S)

12. DISTRIBUTION/AVAILABILITY STATEMENT

Distribution Statement A: Approved for public release; distribution unlimited.

13. SUPPLEMENTARY NOTES

14. ABSTRACT

Report developed under SBIR contract for topic BAA #09-011. The proposed work is in direct support of the Office of Naval Research's Transparent Urban Structures (TUS) program. The objective of the TUS program is to improve the collection, understanding, and dissemination of intelligence for the urban conflict. Through TUS, ONR seeks to develop technology which assists the warfighter in understanding the urban terrain of interest by detecting and classifying threats, both inside buildings and underground, and by maximizing situational awareness inside structures. The key focus of TUS is to develop advanced technologies that make urban man-made structures transparent, thereby eliminating the safe harbor that buildings provide to hostile forces and their malicious activities.

15. SUBJECT TERMS

SBIR Report

16. SECURITY CLASSIFICATION OF:			17. LIMITATION OF ABSTRACT	18. NUMBER OF PAGES	19a. NAME OF RESPONSIBLE PERSON
a. REPORT	b. ABSTRACT	c. THIS PAGE			Martin Kruger
Unclassified	Unclassified	Unclassified	SAR	24	19b. TELEPHONE NUMBER *(Include area code)* (703) 696-5349

Reset

Standard Form 298 (Rev. 8/98)
Prescribed by ANSI Std. Z39.18

Intelligent Automation Incorporated

Coherent distributed radar for high-resolution through-wall imaging

Final Report

Contract No. N00014-10-C-0277

Sponsored by

Office of Naval Research

COTR/TPOC: Martin Kruger

Prepared by

Eric van Doorn, Ph.D. (PI)

Satya Ponnaluri, Ph.D.

Distribution Statement A: Approved for public release; distribution unlimited.

Final report

Contents

Final report 1

1 Summary 2

2 Technical Results 3

2.1 Hardware 3

2.1.1 Reciprocal Transceiver Architecture 3

2.1.2 Lower jitter hardware 4

2.1.3 Jitter measurement methods 5

2.1.4 Networking 5

2.2 Experimental results 5

2.2.1 Synchronization 5

2.2.2 Ranging and Direction Finding 5

2.2.3 Radar imaging with synchronized Master and Slave nodes 12

2.3 Simulations 14

2.3.1 Ranging and Direction Finding 14

2.3.2 Through-wall radar 20

3 Conclusions 24

1 Summary

In this project, Intelligent Automation, Inc. developed an approach to wireless synchronization using RF exchanges between transceivers. The approach was simulated, and design parameters were optimized. The approach for the Synchronization and Ranging Transceiver (SRT) was implemented on a Software Defined Radio (SDR) platform and demonstrated over distances of hundreds of feet and slow mobility, and in indoors and outdoors environments. Using the SRTs,

we also demonstrated synchronization-aided ranging and Direction Finding (DF), and a bi-static radar experiment.

2 Technical Results

2.1 Hardware

In the first weeks of the project we focused on developing an overall plan for design of Synchronization and Ranging Transceiver (SRT) hardware for improved better synchronization. The basis for the design is the SRT developed under the prior effort for ONR in 2009. That hardware achieved synchronization accuracy as low as three times the final desired jitter under certain conditions over 20m outdoor links. To improve performance, the new design broadly addressed four main issues: 1) implement a fully reciprocal signaling scheme, 2) determine some measure of round trip time of flight with sub-clock cycle resolution under conditions of multi-path and mild mobility, 3) correct locally generated clocks with better resolution than integer clock cycles, and 4) improve hardware jitter.

2.1.1 Reciprocal Transceiver Architecture

The basic principle behind SRT is the notion of channel reciprocity, the fact that Maxwell's equations indicate that, for a time-invariant channel, the forward and reverse channels between to RF transceivers are identical. Channel reciprocity implies that by exchanging messages between each other at the same frequency, transceivers can measure the offset between each other's clocks, and hence adjust them to zero clock offset (i.e. to synchronize). Consider two digital half-duplex transceivers, exchanging messages, and each transceiver accurately recording the time of arrival of the received message.

In this case the (known) times of transmission, and the measured times of arrival are related by the following equations1:

$$t_r' = t_t + \Delta t + \Delta TX + OTOF + \Delta RX'$$

$$t_r = t_t' - \Delta t + \Delta TX' + OTOF + \Delta RX$$

Where t_r' is the time of arrival in the right-hand receiver, t_t is the time of transmission in the left-hand receiver, ΔTX is the delay through the transmit chain of the left-hand receiver, $OTOF$ is the One-way Time Of Flight, $\Delta RX'$ the delay through the receive chain in the right-hand receiver, t_r is the time of arrival in the left-hand receiver, t_t' is the time of transmission in the right-hand transceiver, $\Delta TX'$ is the

[1] Note that, for simplicity, we assume here that the clock frequencies in both transceivers are equal, otherwise all primed time delays need to be multiplied with a factor f/f', where f corresponds to the clock frequency for the left-hand transceiver, and f' corresponds to the clock frequency of the right-hand transceiver.

time delay through the transmit chain of the right-hand transceiver, and ΔRX is the time delay through the receive chain of the left-hand transceiver. Here the times of transmission are assumed known, the time delays through transmit and receive trains calibrated out or measured online, and the One-way time Of Flight and clock-offsets the unknowns to be determined. By simple combination of the two equations, the equations for clock offset and OTOF and can be determined:

$$\Delta t = \frac{1}{2}\left((t_r' - t_r) - (t_t - t_t') + (\Delta TX' - \Delta RX') - (\Delta TX - \Delta RX)\right)$$

$$OTOF = \frac{1}{2}\left((t_r' + t_r) - (t_t + t_t') - (\Delta TX' + \Delta RX') - (\Delta TX + \Delta RX)\right)$$

Note that in the equation for the clock offset, the differences of the time delays through RF receive and transmit chains contribute to the clock offset measurement, whereas the sums contribute to the time of flight measurement.

We know that the receiver architecture used for the prior prototype has to change to meet the requirements for the proposed work. Specifically, a key simplification of the existing prototype is that the signals that are exchanged between the master and slave transceivers are not symmetric, i.e. different frequencies are used for phase locking, Master->Slave, as well as for the wideband pulses going between master and slave receivers. We have also investigated the optimal frequency plan for the transceivers. Key considerations are: 1) what frequencies are occupied by the through-wall radars, 2) what frequencies are subject to interference, 3) Compatibility with FCC regulations –if a requirement-, 4) propagation characteristics, and 5) ease of implementation. One key issue is to adjust the timing in master or slave once the required correction has been determined from the round-trip signal exchange and subsequent digital processing. Our final implementation is a half duplex transceiver design in the UHF frequency range. We have retained a Master-Slave Architecture, and extended the MAC to 40 Slaves. That is, up to 41 transceivers can be synchronized at one time.

2.1.2 Lower jitter hardware

A key objective of the current work is to reduce hardware jitter. We have identified a very low phase noise clock which will form the basis of our clock synthesis design. However, it is very expensive and has a long delivery time. We also have identified clocks with somewhat higher phase noise figures. We have investigated how much phase noise can be tolerated in the system clock to meet the jitter specifications. We have designed a low-jitter clock generation circuit, and used it to drive the clocks inherent in a SDR design, such as ADC clock, D/A clock, etc.

2.1.3 Jitter measurement methods

We have surveyed methods and equipment available to measure jitter accurately. We found that adequate performance can be obtained with high-speed, high bandwidth (>1GHz) . We found that using Agilent scopes, a few mV box and the built-in time-delay measurement can be used to measure jitter (both RMS and mean delay) can be measured accurately.

2.1.4 Networking

We use COTS IP radios to connect SRTs. This IP network is used to commission the network, report system diagnostics, and performance metrics.

2.2 Experimental results

2.2.1 Synchronization

Performance testing was performed under static and mobile conditions, and in both indoor, and outdoor, environments. Synchronization accuracy was found adequate in all circumstances.

2.2.2 Ranging and Direction Finding

The range can directly be computed from the One-way Time Of Flight (OTOF) measurements. During this project we evaluated several algorithms to compute OTOF, and algorithms that compute the range directly from the raw RF observables. We processed data collected in different node location configurations for accuracy of the currently implemented (in VHDL) algorithm:

- Outdoor
- Indoor (LOS)
- Indoor (NLOS)

The currently implemented algorithm is an edge detection algorithm, with the threshold fixed to a specific fraction of the detected correlation peak. This algorithm sets the base line performance of the current ranging system. Figure 1 shows the correlation between the actual measured range between the master and the slave and the reported range (One-Time Of Flight, or OTOF) from our system. Our data shows an RMS range error of 2.6 meters for the outdoor case.

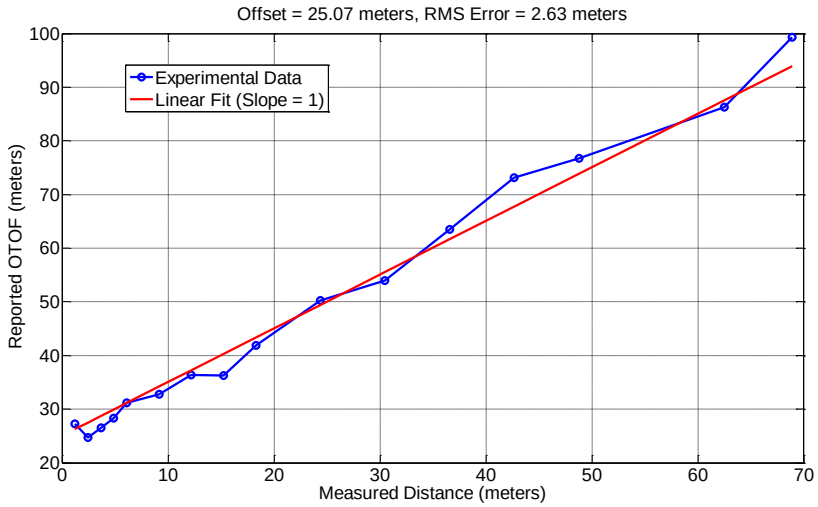

Figure 1. Correlation of measured and reported OTOF data for the outdoor case

We also processed data collected in two indoor configurations: LOS, and NLOS. The correlation between the actual range and reported OTOF for these two subsets are shown separately in Figure 2. This plot shows that for the non-LOS case, the range has an RMS error of 11.7 meters.

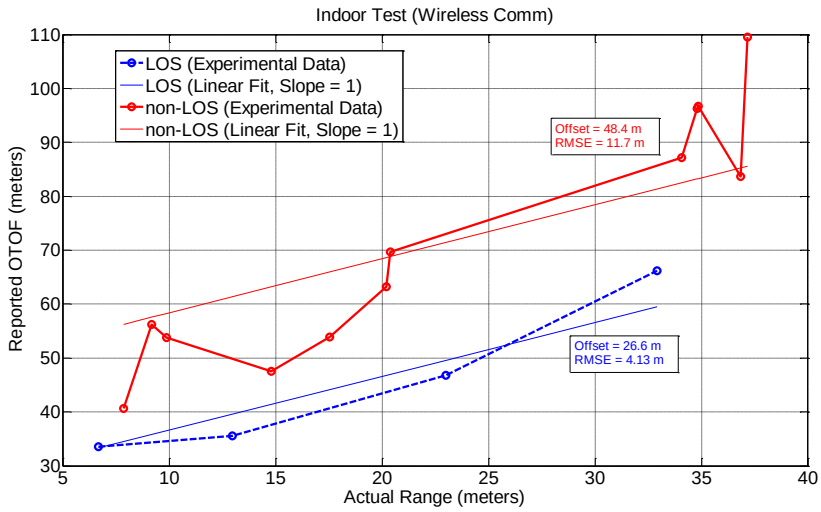

Figure 2. Correlation of measured and reported OTOF data for the indoor case

A second set of data was taken inside the Intelligent Automation building (shown in Figure 3) at similar waypoints. This plot indicates that the system is quite repeatable even for the non-LOS

case when the experiment location is the same. This means the main factor contributing to the range error is multipath, rather than noise or interference.

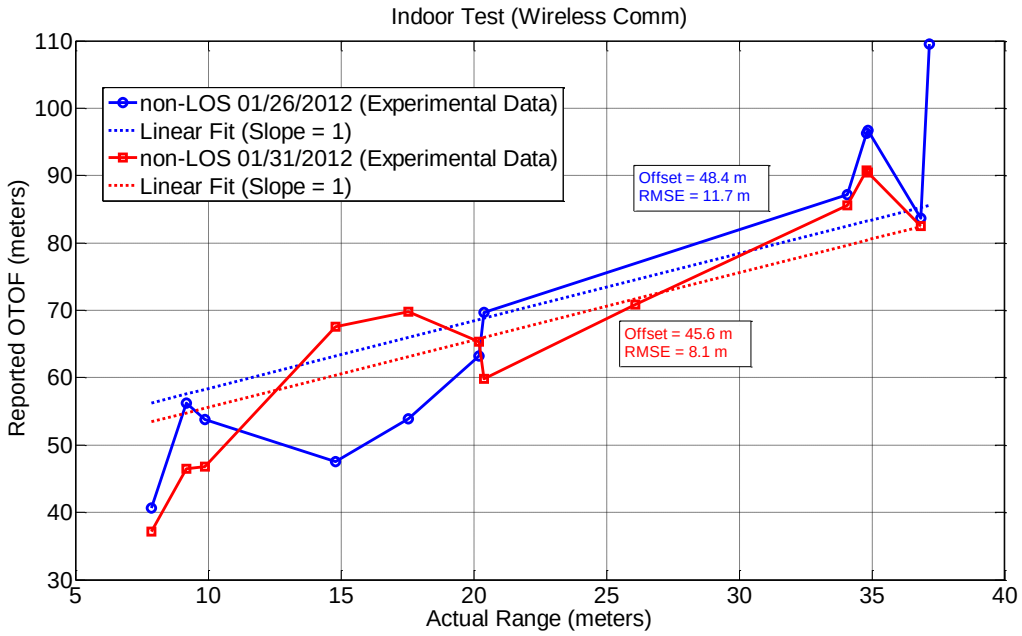

Figure 3. Comparison of two indoor, non-LOS data sets

To facilitate the development and evaluation of ranging algorithms, we enabled the collection of raw data. We configured the hardware and software to stream the complex correlator output at a rate of 10Hz to the PC. This will allow us to evaluate several algorithms for RF ranging offline.

To improve performance, a second edge detection algorithm was designed, implemented and tested. For this algorithm, the raw correlator waveforms were captured, interpolated finely, and a threshold was fixed based on the peak value estimated from the interpolated waveform. Due to better estimation of the peak value, and Time of Arrival estimate, the performance improved significantly. For short range (~200ft) outdoor experiments, we obtain ~60cm accuracy. For indoor experiments, we obtain ~1m accuracy in corridors, and about 6m accuracy for NLOS ranges in an office environment. We show a representative result for a corridor test in Figure 4, below.

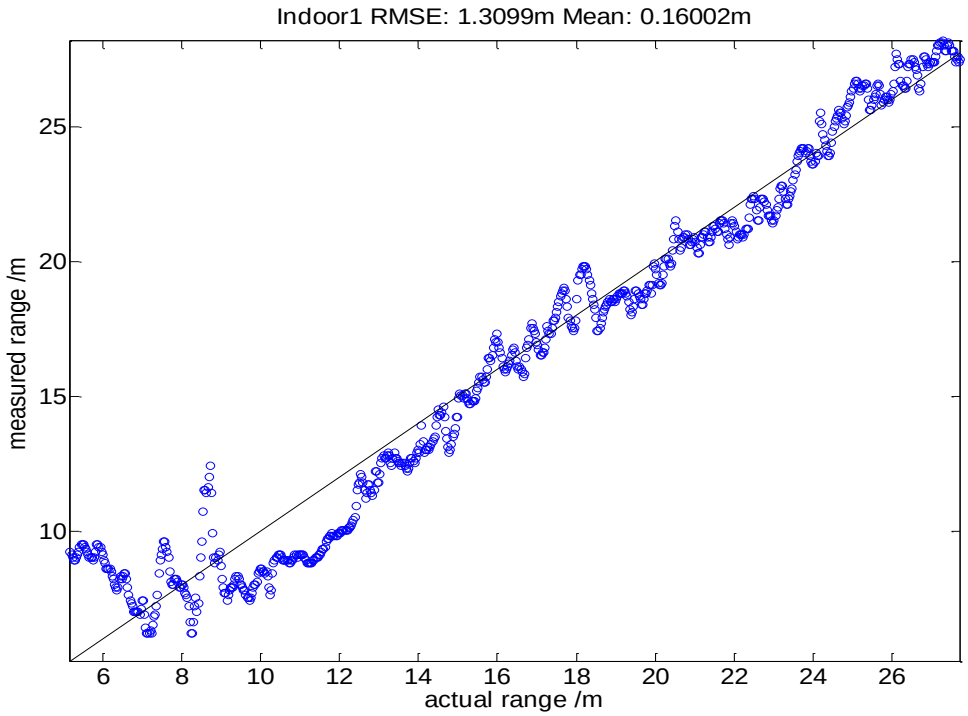

Figure 4. Indoor ranging experiment, office corridor.

2.2.2.1 Beam Forming Ranging

Beam Forming Ranging is an algorithm that attempt to compute a range between transceivers that uses RF samples collected at more than one spatial location. Samples collected multiple positions can be combined in a beam forming algorithm, where the RF data can be combined into signals arriving in a few distinct directions relative to the direction of motion. When multipath reflections are a major source of ranging error, a beam forming algorithm may improve performance as the multipath signal generally arrives from a different direction than the LOS signal.

A key parameter for the beam forming algorithms that is used to improve ranging accuracy (and for imaging) is the aperture: the spatial range over which the multipath environment is sufficiently stationary to be processed coherently. If this aperture is large, a narrow beam can be formed, and multipath can be suppressed effectively. One way to estimate this parameter is to compute the spatial correlation length of the range error. In Figure 5, below, we show the results of an outdoor ranging experiment.

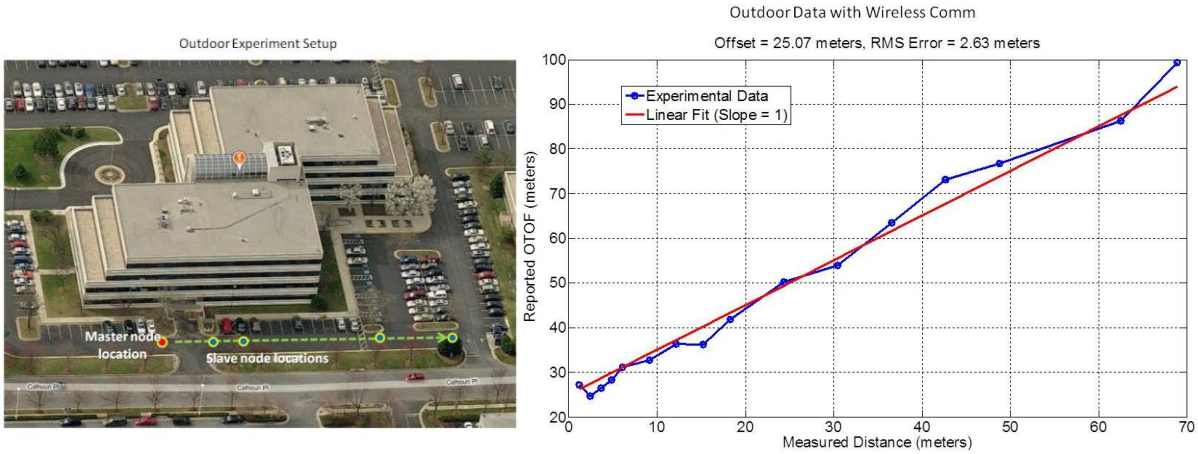

Figure 5. Left: outdoor ranging experiment. Right: reported distance vs. actual distance.

In Figure 6, we show the range error vs. range, and the spatial autocorrelation of the error. The range error de-correlates in about 10m.

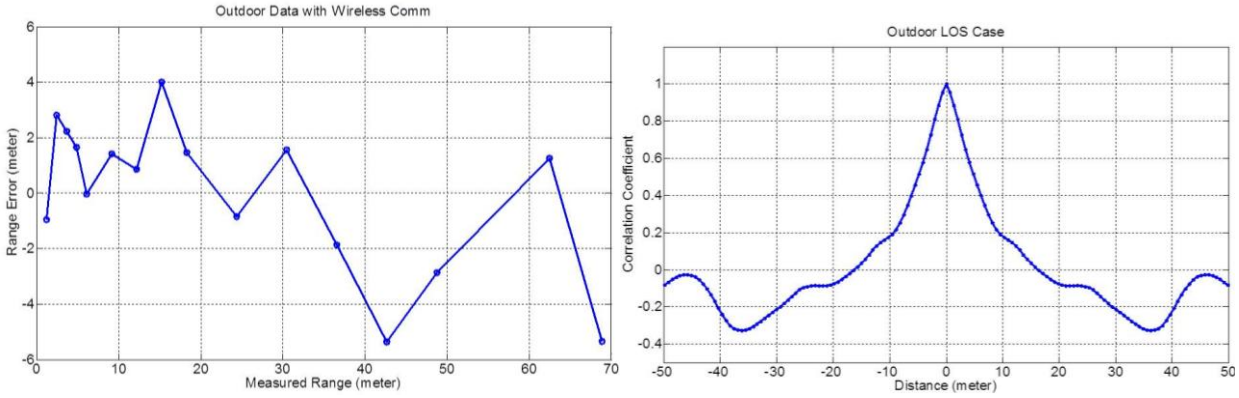

Figure 6. Left: Range error vs. range. Right: Spatial autocorrelation of range measurement.

These results are specific to the particular outdoor environment; carrier, bandwidth, and ranging algorithm used here, but suggest that an aperture of several wavelengths is possible. With beamforming measurements spaced at roughly half wavelength, the potential for beam forming is present.

For an indoors environment, due to the higher density of scatters, the error de-correlates faster, and hence the aperture will be smaller, reducing the potential for beam forming to improve the range accuracy. We show the autocorrelation plots for an indoor office environment below.

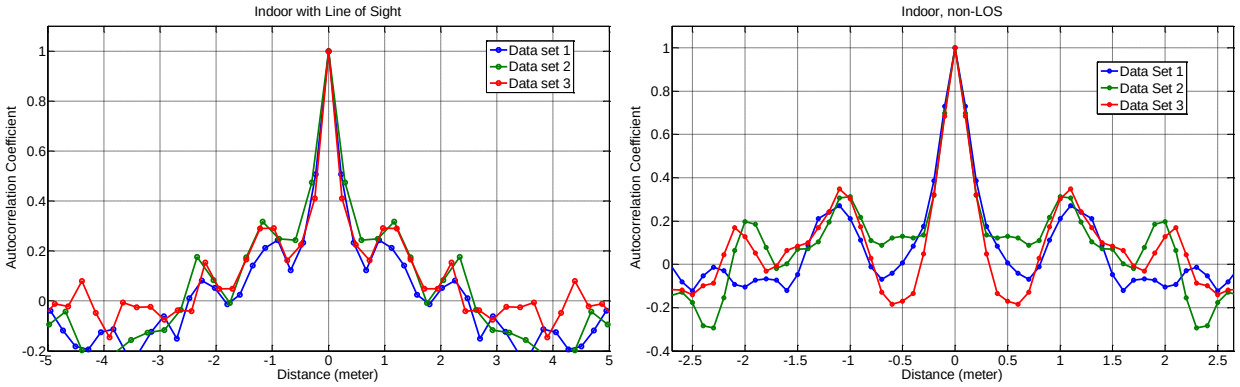

Figure 7. Autocorrelation of range measurement. Left: indoor environment with LOS (corridor). Right: indoor environment without LOS.

For the indoor environment, the aperture will be reduced to 1-2m, essentially making the beamforming approach, at the used frequencies and bandwidth, not suitable for the indoor environment.

Using the beamforming algorithm, we have evaluated two cases. First, we combined samples in such a way that the beam formed pointed at the direction with the strongest signal. One would expect similar performance to an edge detection algorithm. This was confirmed in experiments. Secondly, we combined samples in such a way that the beam points to the direction of earliest arrival. This algorithm appears to lead to larger RMS error for LOS (which makes sense since strongest signal and LOS may not arrive from same direction). In the case of NLOS (indoors) data, the error was significantly smaller than that of the edge detection algorithms. This warrants further investigation.

We also experimentally investigated the potential of channel estimation approaches to reduce the ranging error. In Figure 8, we show the Correlator output for data with very large positive, or very large negative range error.

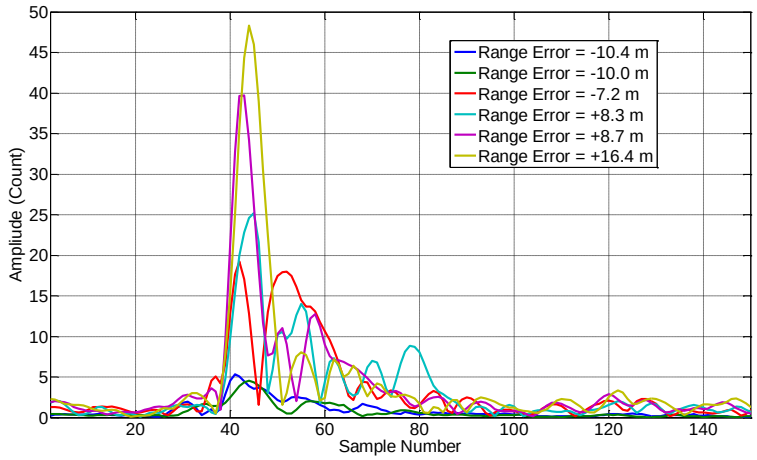

Figure 8. Correlator amplitude vs. sample number for data with various range errors.

The data shows that for large Correlator output, a positive range error is observed, and for small Correlator output, a negative range error output is observed. This result is of course not unexpected; these two cases correspond to constructive and destructive multipath interference respectively. This observation suggests we can improve the range accuracy by methods that are based on channel estimation, such as successive interference cancelation.

2.2.2.2 Direction Finding

We have completed some preliminary experiments using the complex correlator outputs to determine the direction from Slave to Master in the coordinate frame of the Slave. Below we show typical results that indicate that for distances of tens of feet, accuracy on the order of a degree could be obtained.

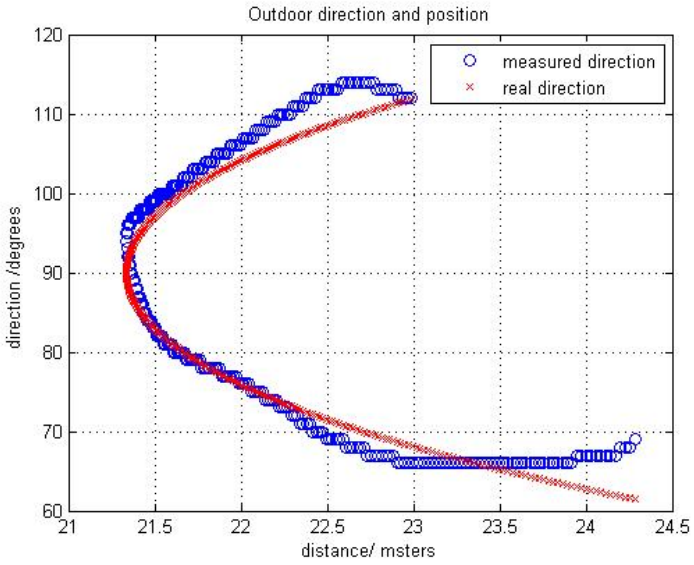

Figure 9. Direction in degrees vs. distance in meters for measured and actual direction.

2.2.3 Radar imaging with synchronized Master and Slave nodes

Besides ranging, tight synchronization between transceivers also enables multistatic radar architectures. In this project, we implemented a bi-static radar concept. Specifically, after synchronizing, we fix the slave node, and move the master node smoothly, collecting raw correlator output continuously. From the starting and stopping time of the master motion, and the known distance, we estimate the relative master and slave positions in 2D (Figure 10). These positions, and the correlator outputs are combined in a backprojection algorithm to form a radar image of the surroundings (Figure 11).

Figure 10. Locations of Master and Slave nodes.

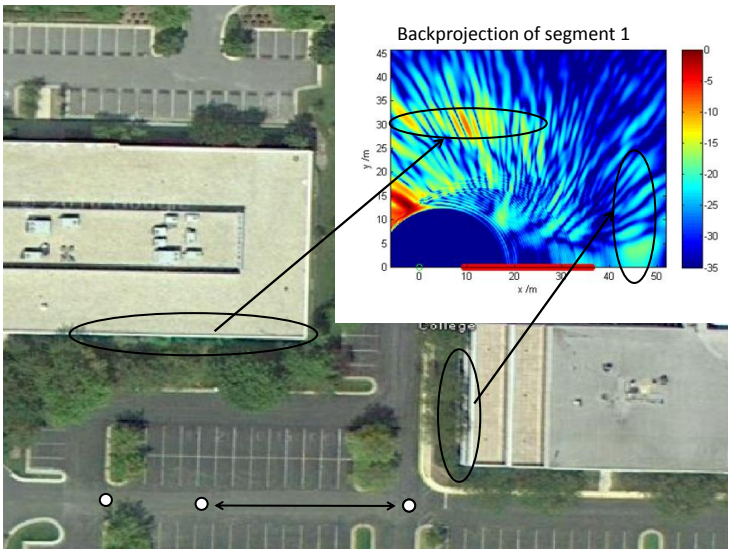

Figure 11. resulting back projection image, and identified scatterers in the image.

Naturally, the image resolution is limited by the bandwidth. In this performance period, we have processed data for radar imaging. Data were taken near two buildings 15400 Calhoun Drive. Both data sets were processed using a coherent back projection algorithm. We show one of the outdoor testing scenarios in Figure 12. The other scenario is similar, but taken near the next building over.

Figure 12. Outdoor testing scenario 1.

We show the back projection imaging results in Figure 13 below. We suspect the bright features in the images correspond to the reflection of the nearby building. We are confirming this suspicion with additional experiments at different distances from the building.

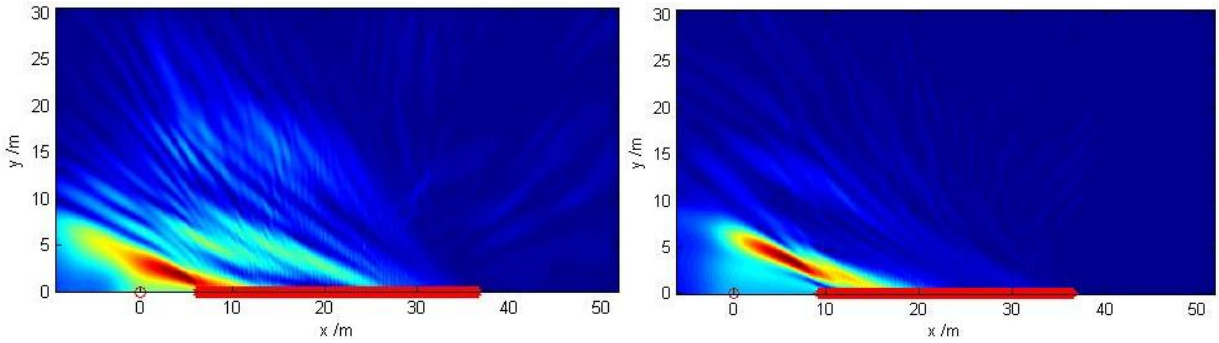

Figure 13. Back projection images for scenarios 1 and 2.

Next, we performed experiments to see if human intruders maybe detected. The experimental procedure was similar. Below, we show representative results. It is clear measurable reflections from the human intruder are observed.

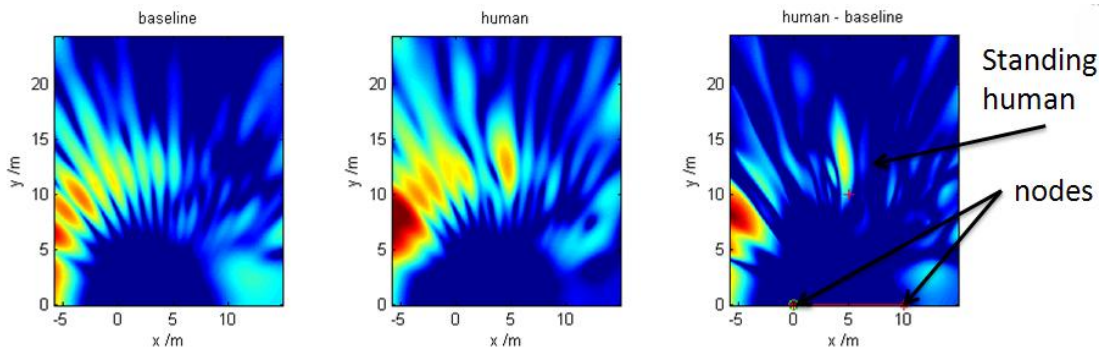

Figure 14. Bi-static SAR data.

We also performed several experiments where the intruder is located within an office building. Here the SRTs are located approximately 50ft away from the outer wall, and the intruder is several feet behind the interior wall. We show representative results below. A combination of range gating and thresholding can be used to detect and locate the human intruder.

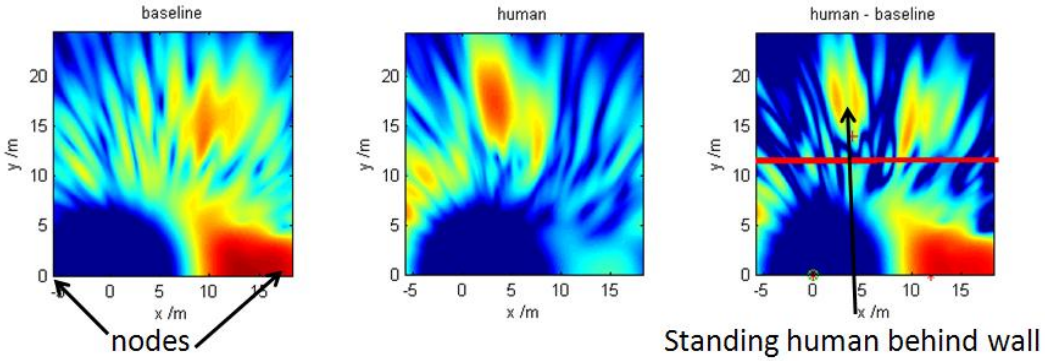

2.3 Simulations

2.3.1 Ranging and Direction Finding

We have performed simulations to study the use of wireless synchronization to improve ranging accuracy in the presence of multipath. Suppose we have a Synchronization Transceiver (ST) equipped with IMU move to sample a wide aperture, and a static ST in a nearby location, in a indoor environment. In this case, receiver beamforming can be used to steer the synthetic beam toward the transmitter for improved ranging, i.e. suppress multipath interference. Furthermore, steering the beam around can also identify multipath scatterers, e.g. walls.

Specifically, we assume 1) the receiver moves to different locations at different times, 2) the IMU records receiver relative position changes, and 3)the receiver performs Digital beamforming. We also study the application of MUSIC for more accurate Direction Of Arrival (DOA) Estimation (DOA)

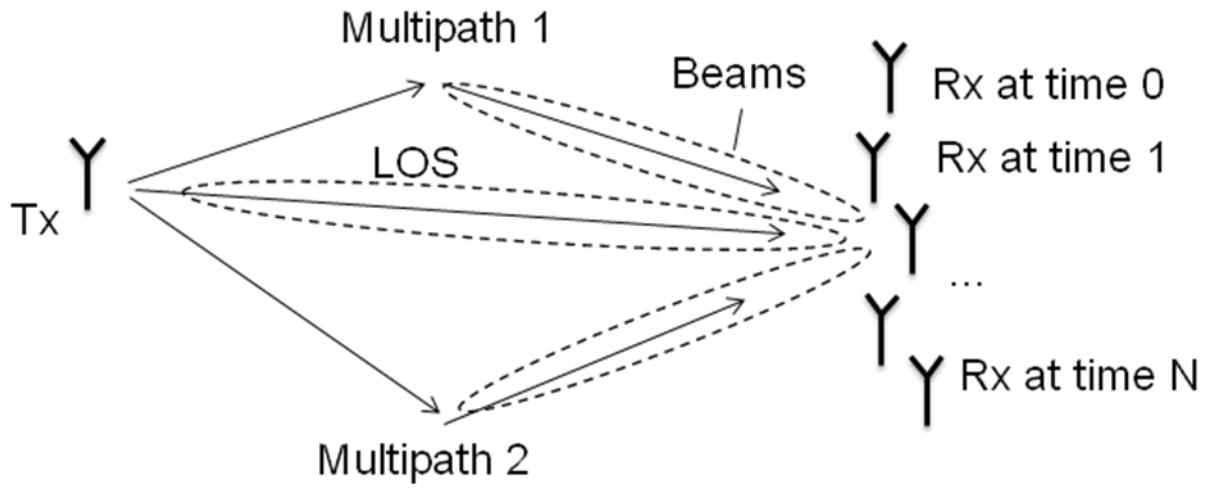

Figure 15. RF ranging between Synchronization Transceivers in a multipath environment.

We are performing simulations to study use of wireless synchronization to improve ranging accuracy in the presence of multipath. Specifically, we are simulating RF ranging in a corridor, where the transmitter and receiver are located at the opposite ends of a 10m long, 5m wide corridor. The receiver moves across a 4m aperture, while recording waveforms. We use a Physic Optics (PO) model to calculate multipath scattering from wall. The LFM waveform has 50MHz of bandwidth @ UHF, and we assume 10dB SNR.

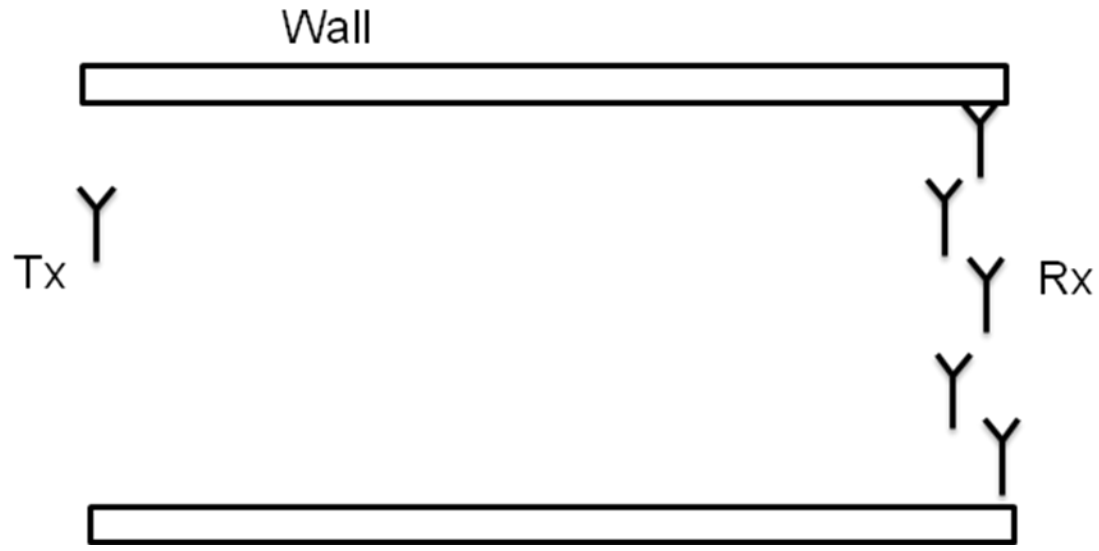

Figure 16. RF ranging in corridor.

We show the received RF signal with and without beamforming in the figure below.

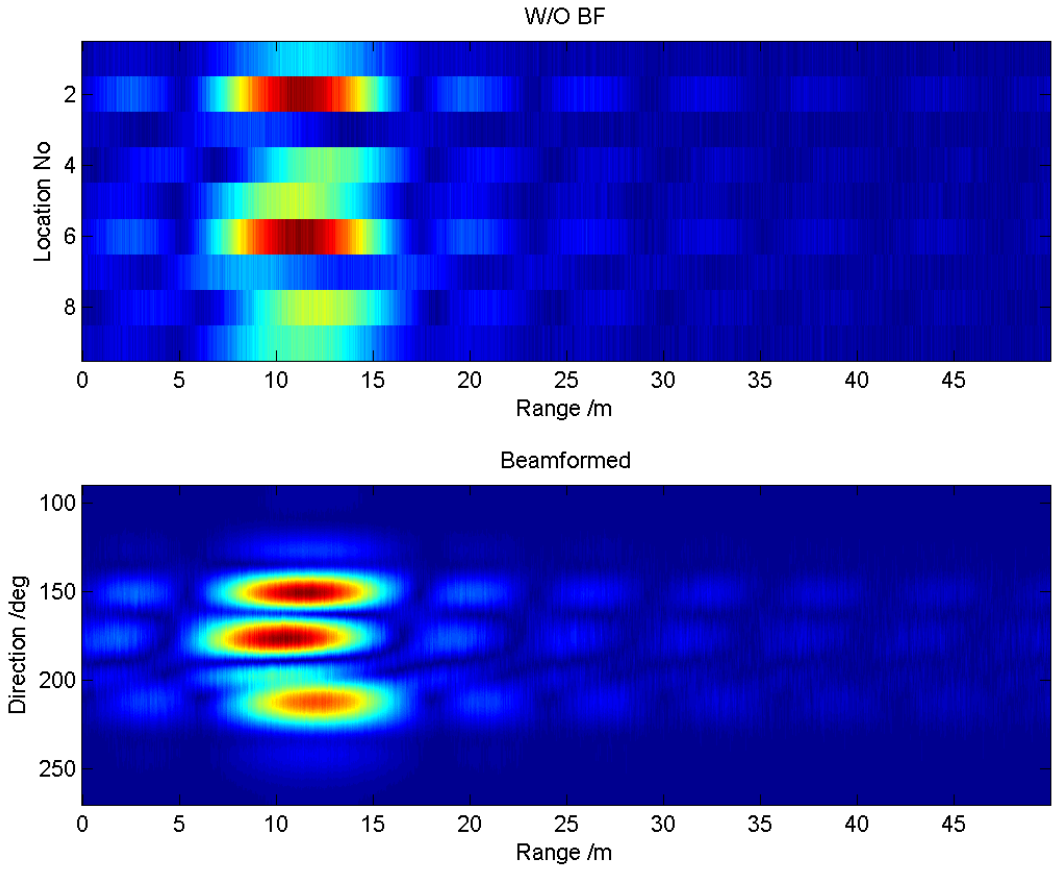

Figure 17. Top: Received signal w/o beam forming. Bottom: with beamforming.

Note that after beamforming, the Line Of Sigh (LOS) and multipath can clearly be distinguished. This forms the basis for the expected improved ranging performance using beamforming.We use MUSIC to find the directions of different signals (LOS and multipath). After beamforming, we determine the range (is equivalent time of arrival for synchronized transceivers) of each signal. We assume the LOS signal corresponds to the signal with the minimum range.

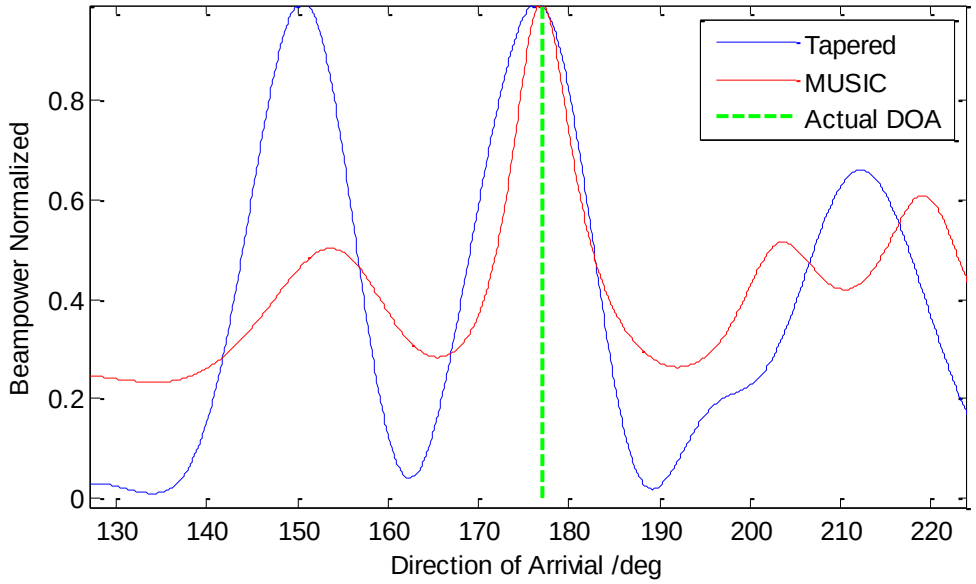

Figure 18. Beam forming results for tapered, and MUSIC.

The beamforming results show that MUSIC improves the DOA accuracy significantly.

2.3.1.1 Estimation of range

In the figure below, we show the resulting range errors with and without beamforming. When we don't use beamforming, we simply average the ranges obtained at the different receiver locations. We find an error of approximately 74cm. With beamforming, we report the range corresponding to the estimated LOS DOA. In this case the error reduces to 5cm.

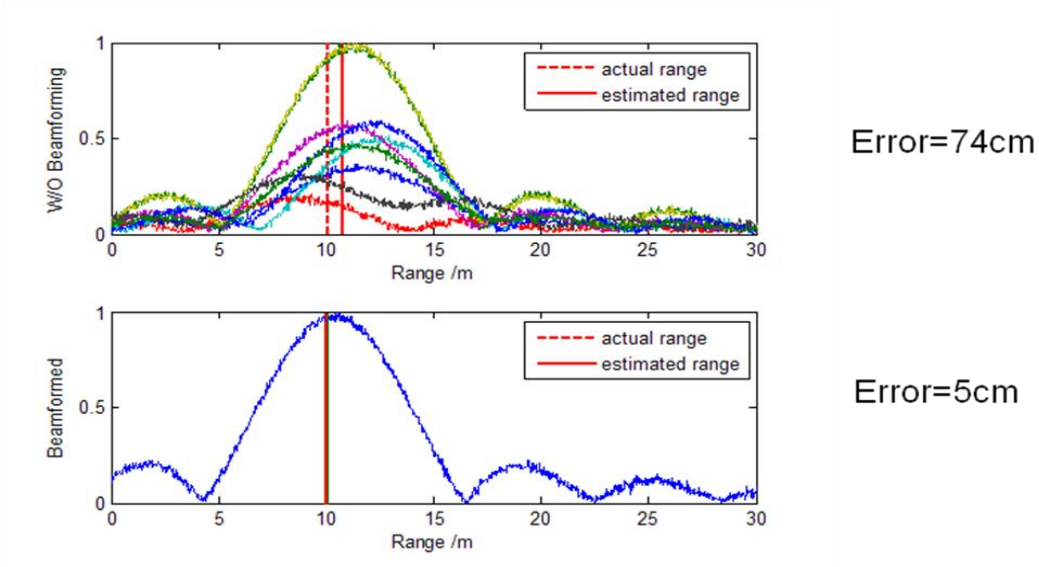

Figure 19. Range accuracy with and without beamforming.

We have also considered ranging using blind beamforming. Blind beamforming is where the receiver moves to different positions during ranging to increase the aperture, but the relative displacement is unknown to the receiver. Here we assume constant spacing between measurements which is smaller than half the carrier wavelength. For instance, if the carrier frequency is 900MHz, and the speed is 1m/s, we assume 6 or more range measurements per second. We simulate two cases.

Case 1: spacing λ/2; direction 12 o'clock, Case 2: spacing λ/4; direction 11 o'clock

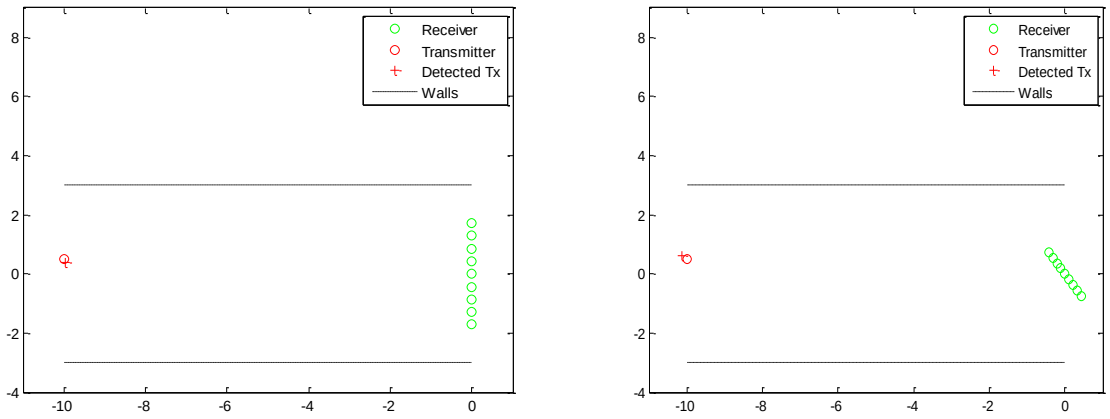

Figure 20. Simulated scenarios.

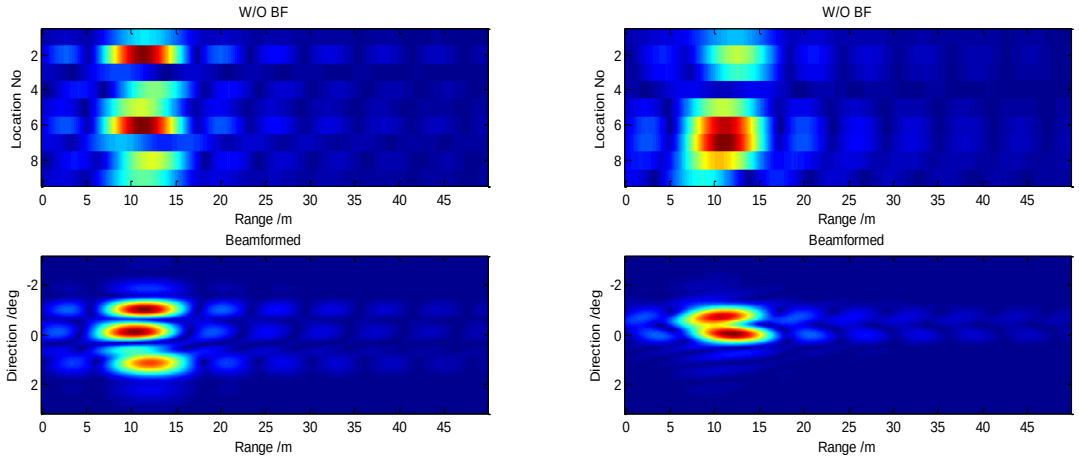

Figure 21. raw signal original vs. Beamformed. Left: Case I. Right: Case 2.

We show the results for direction finding below.

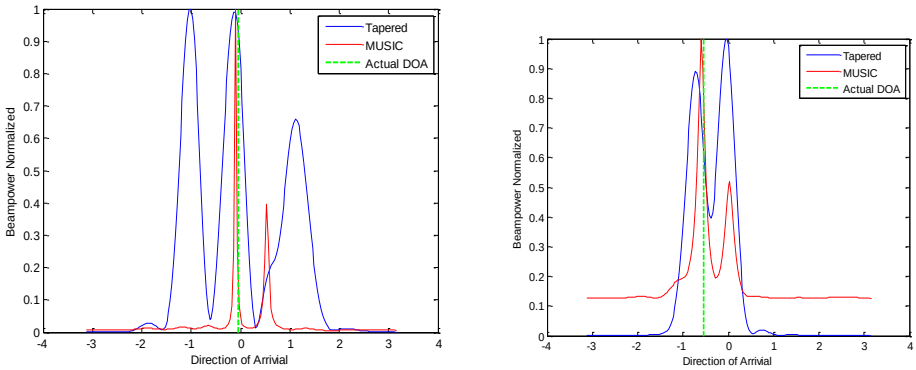

Figure 22. Direction Finding results.

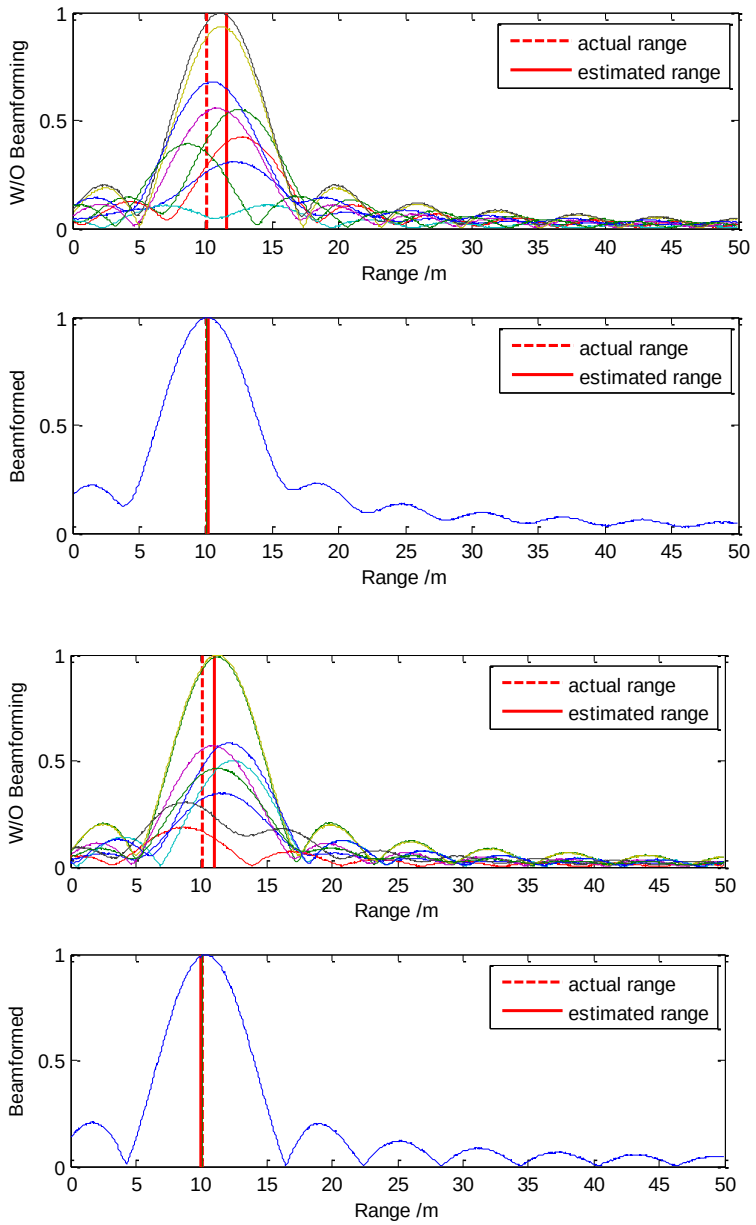

Figure 23. Results for ranging error. Top: Case 1, bottom: case2.

We show the results for ranging with beamforming in the figure above. We conclude that improvement of ranging can be achieved in both cases. This means that ranging accuracy with our synchronization transceiver, under the assumptions of mild acceleration, could be significantly improved by using digital beamforming techniques.

2.3.2 Through-wall radar

In an ARL report [Martone, 2009], a typical through-wall imaging radar is presented. This ARL ground-based, Synchronous Impulse Reconstruction (SIR) radar system is an impulse-based,

ultra-wideband (UWB) imaging radar with a bandwidth covering 300MHz to 3GHz. It employs a physical aperture of 16 receiver antennas. These antennas are equally spaced across a linear aperture that is approximately 2 m long. Two impulse transmitters are located at either end and slightly above the receive array, as illustrated in Figure 24.

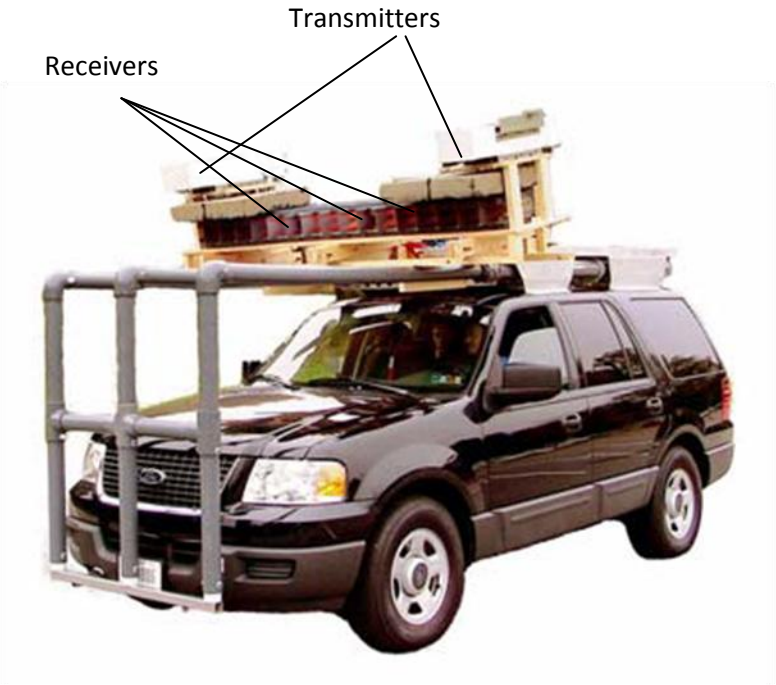

Figure 24 ARL's ground-based UWB radar: SIRE.

The transmitters fire in an alternating sequence—the left transmitter followed by the right. Each transmitter launches a sequence of low-power pulses, and reflected energy is integrated within each receive channel to achieve an acceptable signal-to-noise ratio (SNR). The SIRE radar constructs a high-resolution (0.056 m) downrange profile. This is determined by the bandwidth of the system, i.e.

$$r_R = \frac{c}{2B}$$

Simply employing the back-projection algorithm, 2D Synthetic Aperture Radar (SAR) images can be focused by coherently overlapping the 1D range profiles into the 2D imaging space. According to SAR principles, the resolution in cross-range dimension is determined by the synthetic aperture size which can be approximately estimated as

$$r_A = \frac{\lambda}{2\theta} = \frac{\lambda R}{2L}$$

where R is the range of the imaging area, L is the synthetic aperture size, and θ is the equivalent span of viewing angle.

In the case discussed in this report [Martone, 2009], the imaging area extends from approximately 10 to 35 m. Therefore, we consider $R = 20m$, which yields cross-range resolution of 0.91m. Note that the cross-range resolution is far worse than range resolution. Fortunately, in most through-wall applications, moving target indication (MTI) techniques are employed to detect moving targets behind wall. The static background clutter is cancelled out. Therefore, MTI capability is not significantly limited by the disparity of range vs. cross-range resolution. Moving targets can always be identified as long as they are separated slightly in range dimension.

2.3.2.1 Extended synthetic aperture

In order to improve cross-range resolution, we have to extend the synthetic aperture size. To show the improvement of cross-range resolution, we simulated SAR images of a scene of 5 point targets. As show in Figure 25, the center target is located 15m away from radar, while the other 4 targets are displaced from the center by 0.5m or 3m in either range or cross-range. Note that direct scattering from the wall is ignored in this simulation.

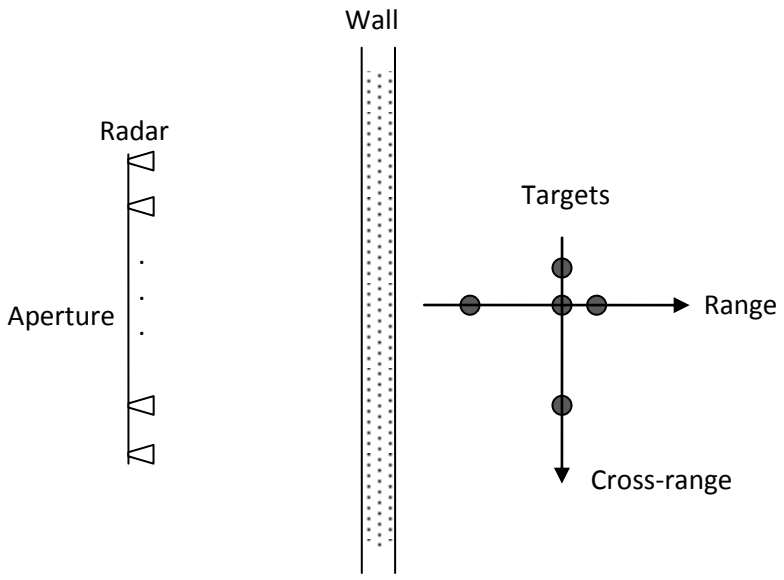

Figure 25 Through-wall SAR image simulation of point targets.

In Figure 26, SAR images of the 5 point targets are shown for the regular 2m-aperture case and an extended 8m-aperture case. Obviously, the first configuration failed to discriminate the two targets displaced by 0.5m in cross-range direction. Also notice that, with extended aperture, even the static SAR without MTI is very informative. In addition to detecting moving target, it could be used to retrieve information about the static scene behind the wall.

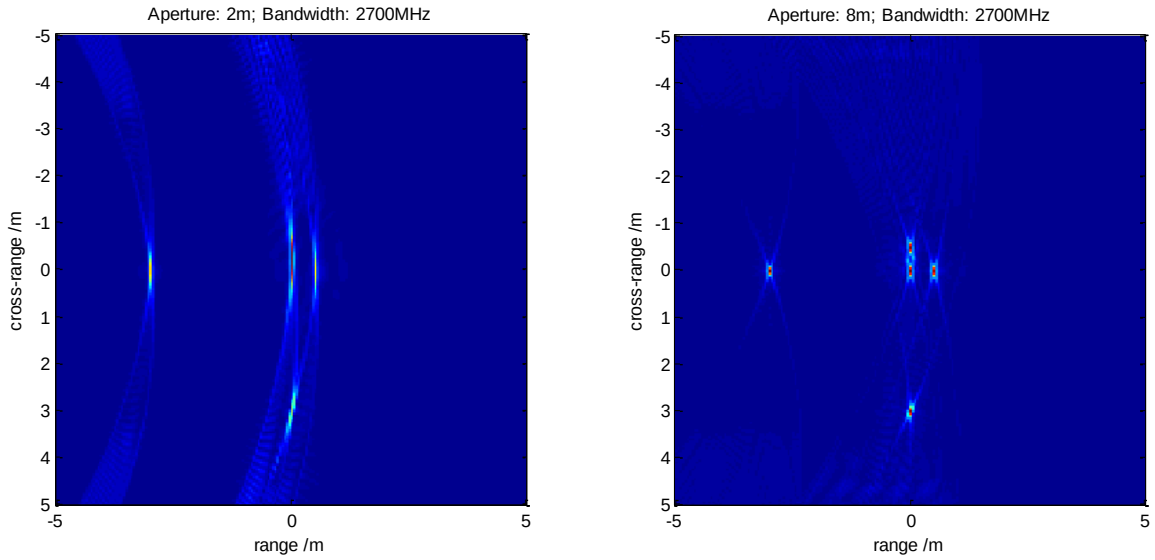

Figure 26 Simulated UWB SAR image with (left) regular aperture and (right) extended aperture.

The aperture size is mainly restricted by the platform size. It is impractical to extend the aperture up to 8m on a ground platform. If we employ a bistatic configuration, such large aperture can be easily achieved by moving a portable receiver around the wall. A static transmitter can be mounted on ground platform, while portable low-power receivers can be carried by person or car. Theoretically, there is no limit of aperture size as the receiver can be moved across as long distance as possible. In practice, the maximum valid synthetic aperture size will be limited by the maximum coherent looking angle, which is the maximum variation of looking angle without losing the coherency in scattering of the target [Ertin, E. et al. 2007].

2.3.2.2 Wide-aperture and narrow-band system

In practice, UWB systems have very limited transmitting power according to FCC regulations under Part 15 (unlicensed band). Exceeding 50microwatts would require the operator to obtain a FCC license before using the system. Given that an extremely wide aperture can be achieved by bistatic portable receiver, system bandwidth maybe reduced without compromising imaging and MTI performance. In that case, the system can be operated in unlicensed band with much larger transmitting power. Two immediate benefits would be longer operating range and avoidance of FCC license application for each user. Below simulation will show how the images look like with wide aperture but limited bandwidth.

The system parameters are the same except using an unlicensed band (bandwidth 80MHz) at 2.4GHz. As shown in Figure 27, with the 8m aperture, the 5 point targets appear to be smeared in range direction and the two targets located too close in range direction are not identifiable. As we further increase the aperture to 24m, we found that all targets become sharper and even the two targets which are close in range direction can now be discriminated. This result indicates that if we employ an extremely large aperture, it is possible to achieve good performance with very

limited system bandwidth, in applications of both MTI and static scene imaging. However, we notice that sidelobes are much higher in narrow-band cases.

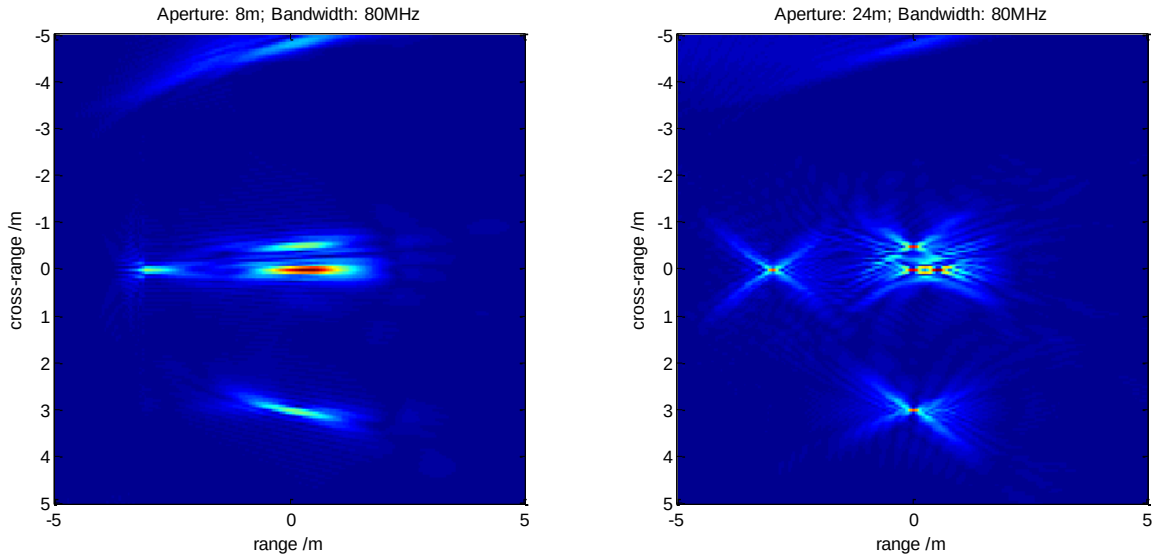

Figure 27 Simulated narrow-band SAR with large apertures.

2.3.2.3 References

Martone, A. et al. (2009): Moving Target Indication for Transparent Urban Structures, ARL report ARL-TR-4809, 2009

Ertin, E. et al. (2007): GOTCHA experience report: three-dimensional SAR imaging with complete circular apertures, Proc. SPIE, Vol. 6568, 656802 (2007); doi:10.1117/12.723245

3 Conclusions

Wireless Synchronization technology has the potential to deliver a revolutionary capability for distributed RF systems. IAI's implementation of SRTs can be readily interfaced to COTS or custom RF transceivers to enable multiple applications, such as emitter localization, pin-point jamming, distributed radar.